Resonant Energy Transfer in the Mixed Crystal Series $[Rh(bpy)_3][NaAl_xCr_{1-x}(ox)_3]ClO_4$ (bpy = 2,2′-bipyridine, ox = Oxalate, $x = 0.05-1$)

Marianne E. von Arx, Vaughan S. Langford, Ueli Oetliker, and Andreas Hauser*

Département de chimie physique, Université de Genève, 30, quai Ernest-Ansermet CH-1211 Geneva 4, Switzerland

Received: January 17, 2002

Efficient resonant energy transfer occurs within the R_1 line of the $^4A_2 \rightarrow {}^2E$ transition of the $[Cr(ox)_3]^{3-}$ chromophore in mixed crystal $[Rh(bpy)_3][NaAl_{1-x}Cr_x(ox)_3]ClO_4$ ($x = 0.05-0.9$, ox = oxalate, bpy = 2,2′-bipyridine). This manifests itself in the form of multiline patterns in resonant fluorescence line narrowing (FLN) experiments at 1.5 K. The conditions for such a resonant process to occur are that the inhomogeneous line width of the R_1 line is larger than the zero-field splitting of the ground state, which, in turn, is larger than the homogeneous line width of the transition. The number of lines and their relative intensities depend critically upon the $[Cr(ox)_3]^{3-}$ concentration and the excitation wavelength within the inhomogeneous distribution. The basic model for resonant energy transfer as presented by von Arx et al. (*Phys. Rev B* **1996**, *54*, 15800) is extended to include the effects of diluting the chromophores in an inert host lattice and of nonresonant R_2 excitation. In addition, Monte Carlo simulations serve to explain the temporal evolution of the multiline pattern following pulsed excitation.

1. Introduction

Recently, we reported on the excitation energy transfer properties of $[Cr(ox)_3]^{3-}$ chromophores in the three-dimensional network structure $[Rh(bpy)_3][NaCr(ox)_3]ClO_4$ (ox = oxalate, bpy = 2,2′-bipyridine).[1,2] At 1.8 K, energy migration within the electronic origin of the low-energy component of the ^2E state, the so-called R_1 line, was shown to be an efficient resonant process. This was, in fact, the first system for which efficient energy migration with clearly resonant character has been reported. In steady-state resonant fluorescence line narrowing (FLN) spectra, this manifests itself in multiline patterns spread across the inhomogeneous distribution, with line spacings equal to the $^4A_2$ ground state zero-field splitting. The quantitative model as presented in ref 2, which assumes a simple set of coupled first order rate equations, gave good agreement between simulated and experimental steady state FLN spectra. For the experimentally observed luminescence decay curves following pulsed excitation, however, there are characteristic deviations at small delays that are in need of a more detailed discussion.

In this paper we present a study on neat $[Rh(bpy)_3][NaCr(ox)_3]ClO_4$ and on the mixed crystal series $[Rh(bpy)_3][NaAl_{1-x}Cr_x(ox)_3]ClO_4$ ($x = 0.05-0.9$). We address the issue of resonant energy migration within the R_1 line of the ^2E state of $[Cr(ox)_3]^{3-}$ in the mixed crystal series including a discussion of the temporal evolution of the multiline pattern following pulsed excitation on the basis of Monte Carlo simulations at 1.8 K. Furthermore, we report on the investigation on lifetime broadening of the R_2 line, the correlation between the R lines, and the consequences for energy migration following irradiation into the R_2 rather than the R_1 line.

* Corresponding author. FAX: (++41) (0)22 702 6103. E-mail: Andreas.Hauser@chiphy.unige.ch

2. Experiment

Polycrystalline samples of neat $[Rh(bpy)_3][NaCr(ox)_3]ClO_4$ and the mixed crystal series $[Rh(bpy)_3][NaAl_{1-x}Cr_x(ox)_3]ClO_4$, with $x = 0.05-0.9$, were prepared as described in refs 3 and 4. For luminescence and excitation spectra a few crystallites were glued to the surface of a copper mount using rubber cement.

Broad band luminescence spectra were obtained by exciting with a cw Ar^+/Kr^+ mixed gas laser (Spectra Physics Stabilite 2108) at wavelengths between 488 and 532 nm, that is, into the $^4A_2 \rightarrow {}^4T_2$ transition of the $[Cr(ox)_3]^{3-}$ chromophore. For fluorescence line narrowing (FLN) experiments on the $^4A_2 \rightarrow {}^2E$ transition, a Ti:sapphire laser (Coherent 899, 2 GHz bandwidth) pumped by a 5 W diode-pumped, frequency-doubled Nd:YVO_4 laser (Coherent Verdi) was used. The luminescence was dispersed by a 0.85 m double monochromator (Spex 1404). A cooled photomultiplier tube (RCA-C31034) was used for detection, and the signal was processed by a gated photon counting system (Stanford Research 400). In the FLN spectra the experimental resolution was limited by the monochromator ($\sim$0.3 cm^{-1} at 20 μm slits). In the resonant FLN experiments the exciting laser beam ($\sim$5 mW, focused) and the resulting luminescence were both passed through the same chopper blade, but with a phase shift of 180° in order to avoid laser light reaching the photomultiplier tube.[5] For time-resolved measurements, a photoelastic modulator (Automates et Automatismes MT0808) was used in addition to the mechanical chopper in order to produce laser pulses of $\sim 1-4$ μs. The time resolved luminescence was recorded using the gated photo counting system at fixed delays for full spectra and a multichannel scaler (Stanford Research 430) for decay curves at fixed wavelengths. For excitation spectra, the Ti:sapphire laser was scanned by a stepper motor at 0.0013 nm (0.027 cm^{-1}) per step in the region of 690−700 nm. Sample temperatures between 1.5 and 4.2 K with the sample sitting in liquid helium were achieved in a

10.1021/jp0201736 CCC: $22.00
Published on Web 07/12/2002

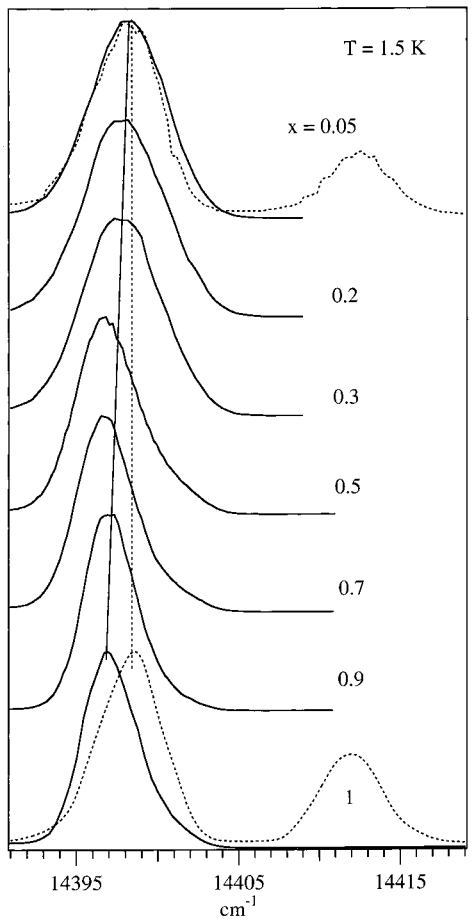

Figure 1. Luminescence (—) and excitation (····) spectra of $[Rh(bpy)_3][NaCr(ox)_3]ClO_4$ at 1.8 K (bottom, adapted from ref 1), and of $[Rh(bpy)_3][NaAl_{1-x}Cr_x(ox)_3]ClO_4$, $x = 0.05$ (top) at 1.5 K, in the region of the ^2E lines. Luminescence spectra: non selective excitation at 543 nm; excitation spectra: broad band detection at 14368 cm^{-1}. Luminescence spectra of the mixed crystal series $[Rh(bpy)_3][NaAl_{1-x}Cr_x(ox)_3]ClO_4$ with $x = 0.2$, 0.3, 0.5, 0.7, and 0.9 at 1.5 K, following nonselective excitation at 543 nm.

pumped He bath cryostat (Oxford Instruments, Optistat Bath) using a home-built manostat.

3. Results

3.1. Nonselective Excitation. Upon excitation into the $^4A_2 \rightarrow {}^4T_2$ absorption band of $[Cr(ox)_3]^{3-}$ in neat $[Rh(bpy)_3][NaCr(ox)_3]ClO_4$ as well as in $[Rh(bpy)_3][NaAl_{1-x}Cr_x(ox)_3]ClO_4$, $x = 0.05-0.9$, the well-known $^2E \rightarrow {}^4A_2$ luminescence[6] is observed, with more than 90% of the total intensity in the electronic origins. At liquid helium temperatures only the so-called R_1 line, that is, only the luminescence from the lower energy component of the zero-field split ^2E state is observed. Figure 1 shows the luminescence spectrum of $[Rh(bpy)_3][NaCr(ox)_3]ClO_4$ at $T = 1.8$ K and the corresponding spectra of the mixed crystal series $[Rh(bpy)_3][NaAl_{1-x}Cr_x(ox)_3]ClO_4$ at $T = 1.5$ K. For $x = 1$ an approximately Gaussian line shape with an emission maximum at ~14396.9 cm^{-1} and with an inhomogeneous line width Γ_{inh} of 3.8 cm^{-1} is obtained. For the systems in the series from $x = 0.9$ down to 0.05, the R_1 line successively becomes somewhat broader and shifts toward slightly higher energies.

For the excitation spectra of the neat compound and the dilute system with $x = 0.05$ shown in Figure 1, the luminescence was detected nonselectively in a vibrational sideband at 14368 cm^{-1}.

TABLE 1: Spectroscopic Parameters for the $^4A_2 \rightarrow {}^2E$ Transition in the Mixed Crystal Series $[Rh(bpy)_3][NaAl_{1-x}Cr_x(ox)_3]ClO_4$, $x = 0.05-1$[a]

x	fwhm lumin.	fwhm excitation Γ_{inh}	red shift[b]	$(N_0(x)/N_0$ $(x = 1))$	further parameters[c]
1.0	3.8 cm^{-1}	4.4 cm^{-1}	1.7 cm^{-1}	1	$\tilde{\nu}_a = 14398.6$ cm^{-1}
0.9	3.9		1.6	0.9	$D(^4A_2) = 1.3$ cm^{-1}
0.8				0.8	$D(^2E) = 13.6$ cm^{-1}
0.7	4.2		1.6	0.7	$k_r = 770$ s^{-1}
0.6				0.57	$\Gamma_{hom} = 0.012$ cm^{-1}
0.5	4.6		1.5	0.47	$k_a/k_b = 2.8$
0.4				0.3	$k_{et'} = 10$ s^{-1}
0.3	5.8		0.8	0.23	
0.2	5.9		0.7	0.15	
0.1				0.08	
0.05	5.7	5.6	0.4	0.04	

[a] These parameters are used for the simulation of the multiline patterns of Figures 2 and 4. [b] Red shift of the R_1 luminescence with respect to the excitation maximum $\tilde{\nu}_a$ of neat $[Rh(bpy)_3][NaCr(ox)_3]ClO_4$. [c] From ref 2.

An approximately Gaussian line shape with its maximum at $\tilde{\nu}_a = 14398.6$ cm^{-1} and an inhomogeneous width $\Gamma_{inh} = 4.4$ cm^{-1} is observed for the R_1 line of the neat compound. This is slightly larger than the 3.8 cm^{-1} observed in luminescence, and with 14398.6 cm^{-1} the maximum is significantly shifted toward higher energies by 1.7 cm^{-1} with respect to the luminescence maximum. This is a first indication that in neat $[Rh(bpy)_3][NaCr(ox)_3]ClO_4$ energy migration is important even at 1.8 K, because at that temperature such a migration tends to concentrate the luminescence at the lower edge of the inhomogeneous distribution. In the excitation spectrum, the maximum of the R_2 line lies at 14411.9 cm^{-1}, and its inhomogeneous line width is ~4.7 cm^{-1}. The zero-field splitting of the ^2E state is thus ~13.3 cm^{-1}, and the ratio of absorption cross sections between the two R lines deduced from the relative intensities is ~0.5. In contrast to neat $[Rh(bpy)_3][NaCr(ox)_3]ClO_4$, the excitation spectrum of the diluted mixed crystal $[Rh(bpy)_3][NaAl_{1-x}Cr_x(ox)_3]ClO_4$, $x = 0.05$, is superimposed upon the corresponding luminescence spectrum, as expected for a system of isolated chromophores.

Within experimental accuracy, the R_1 state of the diluted system is at the same energy than the one for the neat compound in the excitation spectrum, and with 14.3 cm^{-1}, its ^2E splitting is only slightly larger than in the neat compound. In contrast to the shift of the absorption lines, the dilution of $[Cr(ox)_3]^{3-}$ in $[Rh(bpy)_3][NaAl_{1-x}Cr_x(ox)_3]ClO_4$ seems to have a more important effect on the inhomogeneous line width. It is significantly larger for the mixed crystals due to the larger inhomogeneity inherent to mixed crystals. For future reference, Table 1 collects the experimental full widths at half-maximum (fwhm) and the shifts of the R_1 luminescence with respect to the maximum of R_1 excitation line of the neat compound as well as for the series of mixed crystals.

3.2. Fluorescence Line Narrowing. For neat $[Rh(bpy)_3][NaCr(ox)_3]ClO_4$, FLN spectra were recorded at 1.8 K. Upon selective excitation into the R_1 line at various excitation energies $\tilde{\nu}_{ex}$ across the inhomogeneous distribution, the FLN spectra shown in Figure 2 are observed. They consist of multiline patterns with far more lines than the usual three-line FLN spectrum of isolated trigonally distorted Cr^{3+} chromophores.[1,6-8] As discussed in ref 1, such multiline patterns are characteristic for the occurrence of resonant energy transfer. The spacing between adjacent lines $D = 1.3$ cm^{-1} and corresponds to the zero-field splitting of the $^4A_2$ ground state. In contrast to isolated Cr^{3+} chromophores, the resonant line, that is, the line at the exact wavelength of excitation, is not always the most intense,

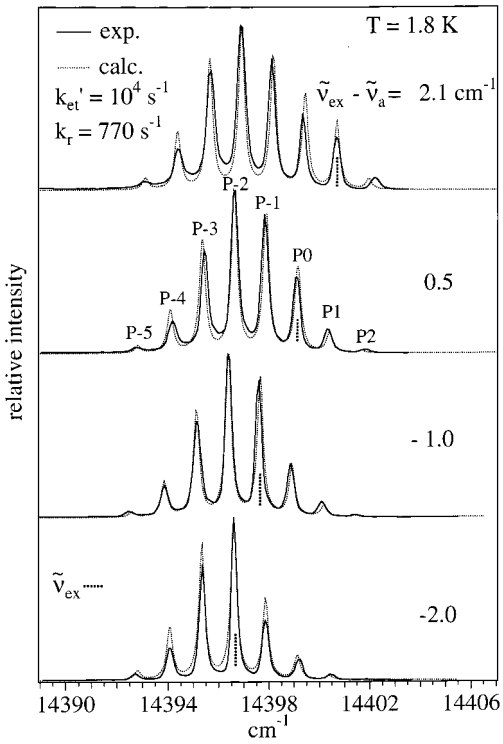

Figure 2. FLN spectra of $[Rh(bpy)_3][NaCr(ox)_3]ClO_4$ at 1.8 K as a function of the laser frequency $\tilde{\nu}_{ex}$ within the inhomogeneous width of the R_1 line (—). Simulated resonant FLN spectra using the relevant parameters for the $[Cr(ox)_3]^{3-}$ chromophore as given in Table 1, and $k_{et}' = 10^4\ s^{-1}$ (••••). $\tilde{\nu}_{ex} - \tilde{\nu}_a$ is the energy difference between excitation energy and the maximum of the R_1 excitation line.

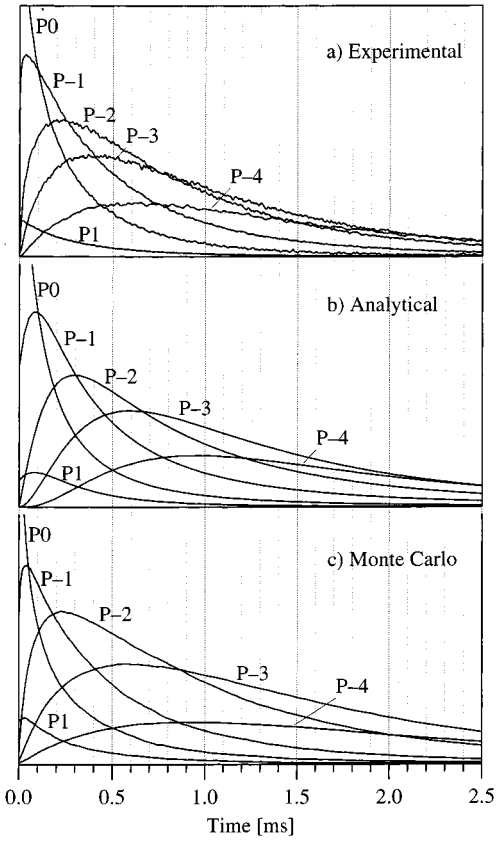

Figure 3. Temporal evolution of the components of the multiline spectrum at $\tilde{\nu}_{ex} - \tilde{\nu}_a = 0.5\ cm^{-1}$ of Figure 2. The resonant line at $\tilde{\nu} = \tilde{\nu}_{ex}$ is labeled with P0. (a) experimental curves, (b) calculated curves using a simple model with one average rate constant, (c) calculated curves obtained from a Monte Carlo simulation taking into account the distribution of rate constants according to the Förster energy transfer mechanism.

in particular for irradiation on the high-energy side of the inhomogeneous distribution. This is due to the efficient energy transfer which, at 1.8 K, takes the system down a ladder toward lower energies. This is further demonstrated by the temporal evolution of the components of the multiline spectrum following pulsed excitation shown in Figure 3a.

The full width at half-maximum (fwhm) of the components of the multiline spectra of Figure 2 is ~0.3 cm^{-1}, that is, it is limited by the experimental resolution. The homogeneous line width itself is expected to be considerably smaller, but unfortunately it is very difficult to determine experimentally for the neat compound. For the system $[Rh(bpy)_3][NaAl_{1-x}Cr_x(ox)_3]ClO_4$, $x = 0.01$, the homogeneous line width has a value of $\Gamma_{hom} \approx 0.012\ cm^{-1}$ at 1.8 K.[1]

Upon selective excitation into the R_2 line at 1.8 K, luminescence from the R_1 state only is expected because of fast thermalization between R_1 and R_2. Figure 4 shows the corresponding FLN spectra in the region of the R_1 line upon excitation at different excitation energies across the R_2 line. Their general behavior strongly resembles the FLN spectra of Figure 2. They, too, show multiline spectra, and the spacing between the lines $D = 1.3\ cm^{-1}$. The number of lines and their intensities also depend critically upon the excitation energy relative to the maximum of the R_2 line in the excitation spectrum. Exciting into the low-energy wing of the inhomogeneous distribution of R_2, only a few lines are obtained. Exciting at higher energies, more lines are observed both at higher and at lower energies with respect to the central line, and also with a bias toward those at lower energies. The central line marked with an asterisk in Figure 4 is defined by the line that is obtained at $\tilde{\nu}_{ex} - D(^2E) = \tilde{\nu}_{ex} - 13.3\ cm^{-1}$. The fwhm of the individual components of the multiline patterns is ~0.6 cm^{-1}, which is larger than the one observed for irradiation into R_1. It is therefore no longer limited by the experimental resolution and may thus be considered real.

In Figure 5, the FLN spectra for irradiation into the R_1 line of the mixed crystal series $[Rh(bpy)_3][NaAl_{1-x}Cr_x(ox)_3]ClO_4$ with $x = 0.05$, 0.1, 0.2 ... 0.9 for different excitation energies within the R_1 line are shown. For the spectra in Figure 5a, the excitation took place at slightly higher energies than the absorption maximum $\tilde{\nu}_a$. For those in Figure 5b, c, the excitation was at around the maximum of the absorption and at lower energy, respectively. The FLN spectra again consist of the multiline patterns, which are the fingerprint for resonant energy transfer. As for the neat component, the spacing between adjacent lines $D = 1.3\ cm^{-1}$ is due to the zero-field splitting of the $^4A_2$ ground state. The number of lines depends strongly upon the chromophore concentration. A smaller concentration of chromophores results in a smaller probability for energy transfer. As a consequence the number of lines observed decreases. Whereas in the more concentrated systems the resonant line is not always the most intense, the resonant line of lower concentrated systems is always the most intense. The FLN spectrum of $x = 0.05$ corresponds almost to the classic three-line spectrum of Cr^{3+} with only a weak additional fourth line at lower energy. The fwhm of the sharp lines is ~0.3 cm^{-1}, which is again limited by the experimental resolution.

4. Discussion

4.1. Energy Transfer within the R_1 Line of $[Cr(ox)_3]^{3-}$. The nature of the energy transfer becomes evident from the FLN

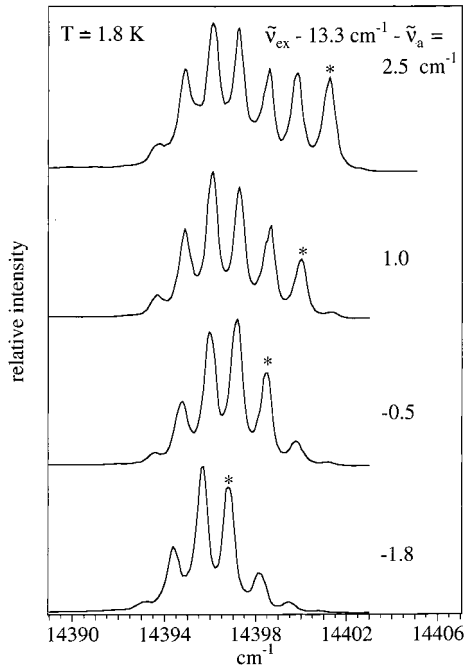

Figure 4. FLN spectra of $[Rh(bpy)_3][NaCr(ox)_3]ClO_4$ at 1.8 K as a function of the laser frequency $\tilde{\nu}_{ex}$ within the inhomogeneous width of the R_2 line. $\tilde{\nu}_{ex} - 13.3\ cm^{-1} - \tilde{\nu}_a$ is the energy difference between excitation energy and the maximum of the R_1 absorption line.

experiment, given in Figures 2 and 5 for the neat compound and the mixed crystal series, respectively. The spectra show multiline patterns at 1.5 K and are characteristic for energy selective and thus resonant energy transfer taking place within the R_1 line of the $[Cr(ox)_3]^{3-}$ chromophores. The requirements for the occurrence of such multiline patterns are that the inhomogeneous line width Γ_{inh} of the transition has to be larger than the zero-field splitting of the ground-state $D(^4A_2)$, which in turn has to be larger than the homogeneous line width Γ_{hom}.[2] In Figure 6, the situation is shown schematically. At $T = 1.5$ K the thermal population of the high-energy component of the zero-field split ground state is not negligible. For clarity, processes due to this thermal population are not explicitly shown, but, with two inhomogeneously broadened and overlapping transitions from the ground state, two sets of molecules are effectively excited at a laser frequency $\tilde{\nu}_{ex}$ within the inhomogeneous envelope: a set for which the transition $g_a \rightarrow e$ is resonant ($\tilde{\nu}_a = \tilde{\nu}_{ex}$), and a set for which the transition $g_b \rightarrow e$ is resonant ($\tilde{\nu}_b = \tilde{\nu}_{ex}$). Resonant energy transfer is, in principle, possible within each of these subsets individually, but because each subset has two possible transitions and because Γ_{inh} is larger than D, additional resonant energy transfer processes become possible. For instance, from the subset $\tilde{\nu}_a = \tilde{\nu}_{ex}$ to the subset at $\tilde{\nu}_a = \tilde{\nu}_{ex} - D$, for which the $g_a \rightarrow e$ transition is resonant with the $g_b \rightarrow e$ transition of the former, or from the subset at $\tilde{\nu}_b = \tilde{\nu}_{ex}$ to the subset at $\tilde{\nu}_b = \tilde{\nu}_{ex} + D$, for which the $g_b \rightarrow e$ transition is resonant with the $g_a \rightarrow e$ transition of the former. This results in a ladder spaced by D within the inhomogeneous distribution, with resonant energy transfer processes between spectral neighbors separated by $\pm D$, and with the hot bands resulting from the thermal population of the high-energy component of the ground state.

Qualitatively, for a given total $[Cr(ox)_3]^{3-}$ concentration, the concentration of resonant $[Cr(ox)_3]^{3-}$ chromophores varies across the inhomogeneous distribution, thus, the average distance between resonant chromophores, and therefore the probability for resonant energy transfer, varies too. Consequently, the structure of the multiline pattern depends strongly upon the excitation frequency. For excitation far into the low-energy tail, there are only a few resonant chromophores, and their distance from each other is so large that hardly any resonant energy

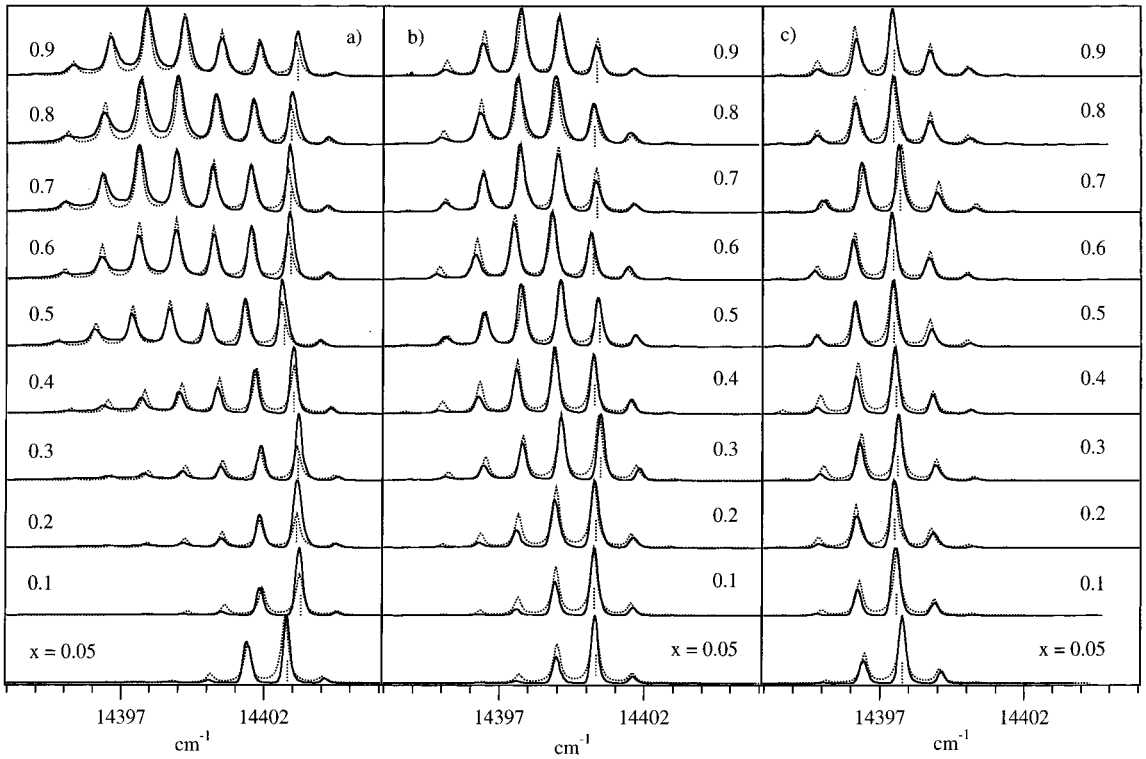

Figure 5. FLN spectra of $[Rh(bpy)_3][NaAl_{1-x}Cr_x(ox)_3]ClO_4$ at 1.5 K as a function of the $[Cr(ox)_3]^{3-}$ concentration x for laser frequencies $\tilde{\nu}_{ex}$ equal to (a) 14401.3 cm^{-1}, (b) 14398.8 cm^{-1}, and (c) 14396.1 cm^{-1}. The energy difference between excitation energy and the maximum of the R_1 absorption line $\tilde{\nu}_{ex} - \tilde{\nu}_a$ is +2.7 cm^{-1}, +0.2 cm^{-1}, and −2.5 cm^{-1} for (a), (b), and (c), respectively. (····) Simulated resonant FLN spectra using the relevant parameters for the $[Cr(ox)_3]^{3-}$ chromophore as given in Table 1 and $k_{et}' = 10^4$ s^{-1}.

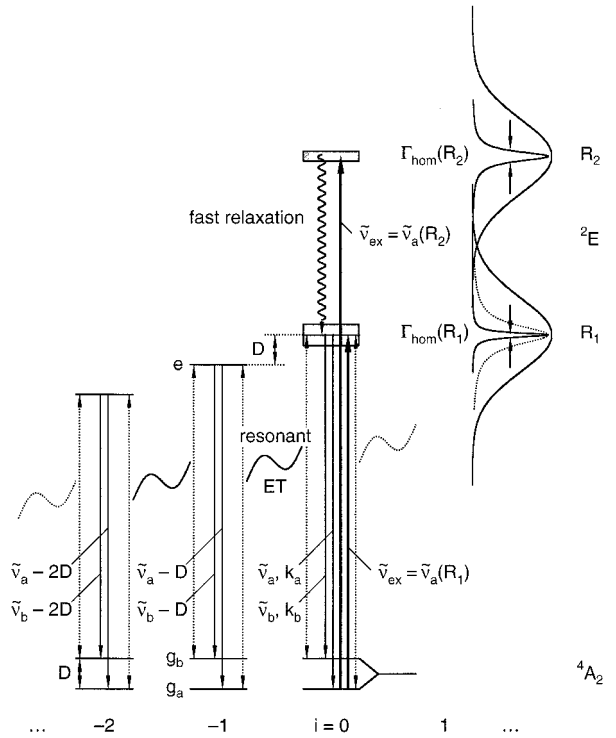

Figure 6. Schematic representation of the processes that occur upon selective excitation into the R_1 or the R_2 line. Parameters are explained in the text. (- - -) Distribution of the lower energy component of the ^2E state following excitation into the R_2 line, taking into account the fact that $\Gamma_{hom}(R_2) > \Gamma_{hom}(R_1)$ and the effect of a nonperfect correlation.

transfer can occur. Thus almost a straightforward three line pattern like in diluted systems is observed. The most striking multiline pattern results for excitation at or near the center of the inhomogeneous distribution, where the concentration of resonant chromophores in subsets of spectral neighbors is comparatively large. Furthermore, at a temperatures of $T = 1.5$ K there is a bias for the resonant energy transfer toward the low-energy subsets of the resonant ladder. In fact, in all spectra in Figures 2 and 5 more peaks are observed at lower energies than at higher energies with respect to the resonant line.

The dependence of the resonant process on the $[Cr(ox)_3]^{3-}$ concentration can be investigated in the series of mixed crystals $[Rh(bpy)_3][NaAl_{1-x}Cr_x(ox)_3]ClO_4$, $x = 0.05-0.9$. The multiline patterns of the FLN spectra in Figure 5 show this concentration dependence. With decreasing $[Cr(ox)_3]^{3-}$ concentration, the concentration of species resonant within a homogeneous line width decreases. As a consequence, the resonant energy transfer becomes less probable, and as a result the number of observed sharp lines is reduced. For the smallest concentration, that is, $x = 0.05$, the FLN spectra for all excitation frequencies resemble the three-line spectrum characteristic for a diluted system with isolated chromophores, with but a barely visible fourth peak on the low-energy side.

Quantitatively, the resonant energy transfer process within the R_1 line can be described by the following set of differential equations for the population of the excited state of the subsets i of complexes giving rise to the different components of the multiline spectra (details see ref 2)

$$\frac{dN_{ei}}{dt} = -N_{ei}(k_r + k_{et}(N_{ai-1} + N_{bi+1})) + k_{et}(N_{ei+1}N_{ai} + N_{ei-1}N_{bi}) + \delta_{0i}\cdot k_a^{ex}\cdot N_{ai} + \delta_{1i}\cdot k_b^{ex}\cdot N_{bi} \quad (1)$$

where N_{ai}, N_{bi}, and N_{ei} are the populations of the three relevant levels in set i (see Figure 6), and k_{et} is to be regarded as an average bimolecular energy transfer rate constant. The third term describes the excitation process of the set labeled $i = 0$ for the transition from the low-energy component of the ground state, and of $i = 1$ for the hot band. The model assumes fast thermalization within the zero-field split ground-state components and negligible spectral hole burning at the excitation wavelength. The latter condition implies that $N_{ei} \ll N_{ai} + N_{bi} = N_{0i}$, where N_{0i} is the number of complexes in the set within a homogeneous line width of the frequency of the ith component of the multiline pattern. The other parameters, for instance the value for the intrinsic decay rate constant k_r of 770 s^{-1} ($\tau_r = 1.3$ ms) and the ratio of the excitation and relaxation rate constants from and to the two components of the ground state k_a^{ex}/k_b^{ex} as obtained for the dilute system $[Rh(bpy)_3][NaAl_{1-x}Cr_x(ox)_3]ClO_4$, $x = 0.01$, are taken from refs 4 and 2, respectively, and are collected in Table 1. Under these conditions, the pseudo first-order rate constant k_{et}', defined as $k_{et}' = k_{et}\cdot N_0$, is the only free parameter, where N_0 is the concentration of acceptors within a homogeneous line width at the maximum of the inhomogeneous distribution. N_0 depends on the total number of equivalent chromophores in the system and the ratio of homogeneous to inhomogeneous line widths as follows

$$N_0 = 2\frac{\Gamma_{hom}}{\Gamma_{inh}}\cdot N_{tot} \quad (2)$$

Here, $N_{tot} = 1.07 \times 10^{21}$ cm^{-3} is the total density of $[M^{III}(ox)_3]^{3-}$ units as calculated from X-ray data.[3] For the neat compound, $N_0 = 6 \times 10^{18}$ cm^{-3}, calculated with $\Gamma_{hom} = 0.012$ cm^{-1} as determined for the diluted system $[Ru(bpy)_3][NaAl_{1-x}Cr_x(ox)_3]$, $x = 0.01$ [1]. In Figure 2, the calculated multiline patterns based on this model, using the experimentally determined value for Γ_{inh} and assuming a Gaussian line shape, are included. The best fit to the observed steady state spectra is obtained for $k_{et}' = 10^4$ s^{-1}. The overall agreement between experimental and calculated spectra is excellent.

Assuming a random distribution of chromophores in the mixed crystal series $[Ru(bpy)_3][NaAl_{1-x}Cr_x(ox)_3]$, $x = 0.05-0.9$, N_0 is the only parameter that changes. It not only scales with x, it is also inversely proportional to the inhomogeneous line width. Taking this into account, the resulting values of $N_0(x)/N_0(x = 1)$ are given in Table 1. In Figure 5, the calculated FLN profiles are included for the full series of $[Cr(ox)_3]^{3-}$ concentrations using the same value for k_{et} as for the neat compound, the appropriate inhomogeneous line width for a given concentration, and the values of $N_0(x)/N_0(x = 1)$ according to Table 1. They are in good agreement with the experimental spectra. Since the probability for resonant energy transfer is reduced in proportion to the decreasing concentration in the manner predicted by the simulations, it may be concluded that the $[Cr(ox)_3]^{3-}$ is indeed randomly distributed in the host material, with no apparent clustering.

It should be noted that the concentration of resonant species is not very high, even for the neat compound, and the fact that even in the most diluted system there is still some remnant resonant energy transfer indicates that it is of long range nature. The only possible interaction mechanism for such long range interaction is, as already discussed in ref 2, a dipole−dipole mechanism. The average bimolecular energy transfer rate constant k_{et} is thus related to the energy transfer probability which, according to the Förster equation,[6] depends on oscillator strengths and spectral overlap integrals. In ref 2, the corre-

sponding critical distance R_c was estimated to be ~47 Å, based on spectroscopic data. This large value is due to the large spectral overlap integral resulting for two resonant lines with homogeneous line widths of 0.012 cm^{-1}.

4.2. Monte Carlo Simulations. Although the above simple treatment of the rate of energy transfer results in a most satisfactory simulation of the steady state spectra, there is a significant and systematic deviation of the calculated luminescence decay curves from the experimental curves following pulsed excitation. Especially at short times after the pulse, the observed build-up of the luminescence for the components at progressively lower energies is faster than that calculated based on the above approach, as is evident from a comparison of Figures 3a and b. This is due to the fact that in the crystal k_{et} is not constant but is different for every chromophore in the system, because the distribution of acceptors around each excited chromophore is different. For the complex system under consideration with several sequential donor−acceptor transfer steps, it is virtually impossible to develop analytical expressions for the temporal evolution of the concentration of the large number of species involved. The often used Inokuti-Hirayama equation[10] is not applicable in the present case of a very noncontinuous distribution of acceptors around a given donor due to the specific crystal structure of the three-dimensional oxalate networks[4] and the shell model as developed in an analytical form by Vasquez and Flint[11] is not adapted to the present problem of sequential processes. The method of choice is clearly a method based on a Monte Carlo algorithm.[12]

The basic idea behind our Monte Carlo algorithm is to follow the history of individual excitations while keeping track of the excited state populations N_{ei} of the subsets at all times. Thus at time $t = 0$, a single chromophore is considered to be excited. Around this chromophore, an acceptor configuration is generated in a random way according to the population numbers of potential acceptors taking into account the actual crystal structure. For all the possible energy transfer processes of this configuration the rate constants are calculated based on the distance to the initially excited ion according to the Förster equation $k_{AD} = \tau_D^{-1}(R_c/R_{AD})^6$, where τ_D is the intrinsic lifetime of the donor, namely 1.3 ms. Of course, the sum of all energy transfer rate constants plus the intrinsic decay rate constant gives the overall decay rate constant for the donor with the given acceptor configuration. Naturally, a Monte Carlo procedure on this configuration results in an exponential distribution of effective life spans from $t = 0$ of the donor according to the overall decay rate constant, but in addition each life span can be attributed to an individual process, that is, energy transfer to a specific acceptor in the configuration or decay by luminescence. For each acceptor having been excited via an energy transfer process and which now acts as donor in subsequent processes, the same procedure of generating an acceptor configuration may now be adopted. The daughter processes, however, have life spans that do not start at $t = 0$ but rather at starting times corresponding to the ending times of the parent process. This can be continued until all excitations have ended in a radiative decay process. From all the life spans, the excited-state populations of the different sets, N_{ei}, at any given moment can be obtained by summing up all sites that are excited at this moment. From this it is straightforward to calculate the luminescence intensity of the peaks P_i of the multiline pattern in the time-resolved spectra at any time after the excitation pulse as well as for continuous irradiation.

In Figure 3c the temporal evolution of the multiline pattern obtained by Monte Carlo simulations is compared with the experimental results and the analytical solutions obtained using the set of differential equations (eq 1). For the simulation, 300,000 primary excitations have been followed. The behavior at the beginning clearly shows a much steeper rise as compared to the analytical solutions and much more in line with the experimental observation. This can be explained by the fact that for configurations with resonant neighbors comparatively close to the initially excited site, energy transfer becomes very fast compared to the average transfer rate. These fast processes even feed sites that need several steps, for example P-3 and P-4, in a very short time.

4.3. Lifetime Broadening and Correlation between R_2 and R_1. The homogeneous line width of the R_1 line in $[Ru(bpy)_3][NaAl_{1-x}Cr_x(ox)_3]$, $x = 0.01$, has been determined to be $\Gamma_{hom} = 0.012$ cm^{-1} (360 MHz) at 1.8 K.[2] In principle, in an FLN experiment the observed line width of the resonant line would be equal to $2\Gamma_{hom}$, provided the laser line width is smaller than Γ_{hom}.[5,6] In the concentrated materials, lifetime broadening due to energy transfer is negligible for the transfer rates under consideration. Nevertheless, each resonant energy transfer step would broaden the observed line width by an additional $2\Gamma_{hom}$. Therefore, the fwhm of the sharp lines of ~0.3 cm^{-1} of the FLN spectra with excitation into R_1, shown in Figure 2, is clearly given by the experimental resolution of our setup even for those members of the series of lines far away from the central line.

Generally, Γ_{hom} of any transition is given by[14−16]

$$\Gamma_{hom} = \frac{1}{2\pi T_1} + \frac{1}{\pi T_2^*} = \frac{1}{2\pi T_2} \qquad (3)$$

where T_1 is the lifetime of the excited state and T_2^* is the pure dephasing time. T_2 is called the effective dephasing time. T_1^{-1} is given by the sum of the radiative and the nonradiative decay rate constants, $T_1^{-1} = k_r + k_{nr}$. The pure dephasing time T_2^* is often dominated by quasi-elastic scattering of phonons. In addition, electronic and nuclear spin fluctuations can contribute significantly to the dephasing process. At liquid helium temperatures, there are very few phonons excited, and for electric dipole allowed transitions the dephasing time T_2^* may become long relative to the lifetime T_1 of the excited state. In such a case, Γ_{hom} at low temperature is determined by T_1 only. In the present case of a spin-forbidden d−d transition, T_1 of the R_1 line is 1.3 ms.[1,4] The corresponding contribution to the homogeneous line width is ~120 Hz, which is orders of magnitude smaller than the ~360 MHz observed at 1.8 K. Thus, $\Gamma_{hom}(R_1)$ is determined by the pure dephasing time T_2^* even at 1.8 K. This observation agrees with the experiments on $[Cr(bpy)_3]^{3+}$ doped into $[Rh(bpy)_3](PF_6)_3$, for which a value for $\Gamma_{hom}(R_1)$ of 320 MHz was found.[9]

For selective excitation into the R_2 line, the possible processes are illustrated in Figure 6 (where processes from the hot bands have been omitted for simplicity). Upon excitation of a subset of chromophores out of the inhomogeneously broadened R_2 line, fast relaxation to the R_1 state takes place. Due to the fast thermalization, $\Gamma_{hom}(R_2)$ becomes substantially broader than $\Gamma_{hom}(R_1)$ according to eq 2, and assuming the same value of T_2^* for both R lines.[5,8] Thus, the line width of the luminescence from R_1 following excitation into R_2 is determined basically by $\Gamma_{hom}(R_2)$. For $\Gamma_{hom}(R_2) \gg \Gamma_{hom}(R_1)$ it should, in fact, be equal to the former, provided the correlation of the ^2E splitting across the inhomogeneous distribution is good. Additional broadening can originate from poor correlation between the two R lines. Once in the excited R_1 state, resonant energy transfer within the R_1 line occurs in the same way as for direct R_1 excitation.

Similarly, for $T > 0$, the thermal population of the zero-field split ground state component g_b has to be considered, which results in the excitation of a second subset and which is responsible for resonant energy transfer to subsets at higher energies within the ladder spaced by D.[1,2]

The luminescence spectra following excitation into R_2 transition of neat $[Rh(bpy)_3][NaCr(ox)_3]ClO_4$ at 1.8 K of Figure 4 show multiline patterns that are very similar to the one resulting from direct excitation into R_1. Thus, the correlation of the ^2E splitting must be good, in accordance with the general findings that in well crystallized materials the R lines are often correlated to within 1%.[5,16] The key difference between the spectra of Figure 2 and those of Figure 4 is that for the latter the fwhm of the individual peaks is 0.6 cm^{-1} and is thus no longer limited by the experimental resolution. Excluding correlation losses, this value gives an upper limit for $\Gamma_{hom}(R_2)$. The value of 0.6 cm^{-1} for $\Gamma_{hom}(R_2)$ has to be compared to literature values. For $[Cr(bpy)_3]^{3+}$ doped into $[Rh(bpy)_3](PF_6)_3$, Riesen [9] found a corresponding value of 1.8 cm^{-1} at 1.5 K, from which a relaxation rate constant for the $R_2 \rightarrow R_1$ relaxation of 3.4×10^{11} s^{-1} can be calculated. This is 2 orders of magnitude faster than observed in Al_2O_3 doped with Cr^{3+} (ruby),[17] and has been attributed to the higher density of low-energy vibrational states of the $[Rh(bpy)_3](PF_6)_3$ host as compared to ruby. For our title compound with the quite rigid oxalate lattice, the phonon density of states is expected to be somewhat lower than for $[Rh(bpy)_3](PF_6)_3$, but still very much closer to this compound than to ruby. The value of $\Gamma_{hom}(R_2)$ of 0.6 cm^{-1} with the corresponding relaxation rate constant of 10^{11} s^{-1} agrees with this expectation.

Taking into account this large value for the $R_2 \rightarrow R_1$ relaxation rate constant, energy transfer taking place within the R_2 line before relaxation to the R_1 state can be excluded. Thus, the multiline patterns in Figure 4 are definitely due to resonant energy transfer within the R_1 line only. Since, at 1.8 K hardly any phonon-assisted energy transfer is observed, the background of the nonresonant multiline spectra is mainly due to the Lorentzian long tails of the lifetime broadened lines. Of course, some small correlation losses cannot be excluded at this stage. Only for excitation into the high-energy wing of the R_2 line can the resulting background in the FLN spectra be attributed to some phonon-assisted energy transfer, as it is also seen in the FLN spectra with excitation into the high energy wing of the R_1 line.

5. Conclusions

A prerequisite for the observation of resonant energy migration within the electronic origins of the R_1 line is a high concentration of chromophores without having them interact with each other via a superexchange mechanism. The special architecture of the three-dimensional oxalate networks allows such a high concentration of the photophysically active chromophore. At the same time it prevents the formation of exchange-coupled pairs, as by virtue of the synthetic procedure,[3] there is always an inert sodium ion between the trivalent chromium ions. In addition, in order for the multiline pattern to be observable, the homogeneous line width has to be smaller than the zero-field splitting of the ground state, which in turn has to be smaller than the inhomogeneous line width. This condition is perfectly fulfilled in the oxalate networks. A key question to be addressed in the future regards the homogeneous line width, which so far has been determined only for the very dilute system and need not be the same in the more concentrated systems due to additional dephasing processes. It is, however, a central parameter as it determines both the Förster radius as well as the concentration of resonant species. This point should and will be clarified using transient hole burning techniques.

Acknowledgment. We thank Nahid Amstutz of the Université de Genève for the preparation of samples. This work was financially supported by the Swiss National Science Foundation.

References and Notes

(1) Hauser, A.; Riesen, H.; Pellaux, R.; Decurtins, S. *Chem. Phys. Lett.* **1996**, *261*, 313.
(2) von Arx, M. E.; Hauser, A.; Riesen, H.; Pellaux, R.; Decurtins, S. *Phys. Rev. B* **1996**, *54*, 15800.
(3) Decurtins, S.; Schmalle, H. W.; Pellaux, R.; Schneuwly, P.; Hauser, A. *Inorg. Chem.* **1996**, 35, 1451.
(4) Langford, V. S.; von Arx, M. E.; Hauser, A. *J. Phys. Chem. A* **1999**, *103*, 7161.
(5) Riesen, H.; Krausz, E. R. *Comments Inorg. Chem.* **1993**, *14*, 323.
(6) Henderson, B.; Imbusch, G. F. *Optical Spectroscopy of Inorganic Solids*; Clarendon Press: Oxford, 1989; p 469.
(7) Szabo, A. *Phys. Rev. Lett.* **1971**, *27*, 323.
(8) Imbusch, G. F.; Yen, W. M. In *Laser, Spectroscopy and new Ideas*; Yen, W. M., Levenson, M. D., Eds.; Springer Series in Optical Sciences 54; Springer: Berlin, 1987; p. 248.
(9) Riesen, H. *J. Lumin.* **1992**, *54*, 71.
(10) Inokuti, M.; Hirayama, F. *J. Chem. Phys.* **1965**, *43*, 1978.
(11) Vasquez, S. O.; Flint, C. D. *Chem. Phys. Lett.* **1995**, *238*, 378.
(12) Diaz-Torres, L. A.; Barbosa-Garcia, O.; Struck, C. W.; McFarlane, R. A. *J. Lumin.* **1998**, *78*, 69.
(13) Oetliker, U.; Hauser, A. *A Monte Carlo simulation programme for sequential energy transfer*, manuscript in preparation.
(14) Schenzle, A.; Brewer, R. G. *Phys. Rev. A* **1976**, *14*, 1756.
(15) Shimoda, K. In *High-Resolution Laser Spectroscopy*, Topics in Applied Physics, Vol. 13; Shimoda, K., Ed.; Springer-Verlag: Berlin, 1976; p 1.
(16) Krausz, E. R.; Riesen, H. In *Inorganic Electronic Structure and Spectroscopy*, Vol I; Solomon, E. I., Lever, A. B. P., Eds.; Wiley: New York, 1999; Chapter 8, p 307.
(17) Rives, J. E.; Meltzer, R. S. *Phys. Rev. B* **1977**, *16*, 1808.